Experimental and numerical study of a motion amplification mechanism to enhance the seismic dissipation capacity of precast, post-tensioned concrete rocking systems

Ahmet Ata Kulaksizoglu, Cetin Yilmaz, and Cem Yalcin

- The external damper proposed in this research uses the concept of motion amplification, which aims to magnify the seismic displacements and rotations imposed on the joint by the gap-opening mechanism.
- To investigate the behavior of precast, post-tensioned concrete rocking systems with the proposed dampers, a representative frame and 10 subassemblies to obtain the cyclic force-displacement response were analyzed.
- Experiments were conducted on a prototype damper mechanism to investigate the effect of various parameters on the force-displacement response and to verify the numerical modeling principles. Numerical studies of the subassemblies showed that the proposed damper mechanism increased the energy dissipation and force capacity of unbonded, post-tensioned rocking systems.

The modern approach to the seismic design of structures focuses on two main objectives: providing sufficient strength to resist loads caused by earthquake excitation and providing sufficient ductility so that the structure can undergo inelastic deformations without failing in a brittle manner. Inelastic behavior is permitted, and even encouraged, because it is not economically feasible to design structures to remain elastic in an earthquake event. However, inelasticity causes damage in structural members. In many cases, efforts to repair the structural damage and retrofit the structure are expensive and adversely affect the functionality of the structure. Low-damage seismic systems have emerged to address these challenges in buildings. In these types of structural systems, negligible and repairable seismic damage is localized at specially designed locations and residual deformations are reduced.[1]

One type of low-damage seismic system is a precast, post-tensioned concrete frame structure in which lateral load-resisting capacity is provided by precast concrete elements and the post-tensioning tendons that connect them.[1,2] These precast, post-tensioned concrete rocking systems minimize damage in two ways. First, seismic damage is localized at the rocking interface between beams and columns, rather than at the components themselves, because of the gap-opening mechanism that occurs when the structure is subjected to earthquake excitation. This joint is special-

ly designed to minimize the amount of damage. Second, the post-tensioning tendons are designed to remain elastic under seismic demands. Since these tendons are the primary components of the lateral load-resisting system, the system can "self-center" after the earthquake, which reduces residual deformations dramatically. Priestley et al.[1] have demonstrated that at large drift demands, the amount of damage in reinforced concrete buildings is considerably greater than the level in buildings with precast and post-tensioned concrete rocking systems.

These distinctive features of precast, post-tensioned concrete rocking systems also have disadvantages. The lack of plastic hinging in the components of these systems, along with the elastic design of the post-tensioning tendons, limits the hysteretic energy dissipation capacity that is inherent in conventional reinforced concrete structures. As a result, the lateral displacement demands may be greater than what is acceptable for these systems. In the first generation of comprehensive experiments studying the behavior of precast and post-tensioned concrete, mild steel reinforcement was placed at the top and bottom parts of the beam to enhance energy dissipation capacity.[2] However, if mild steel reinforcement is used to contribute to hysteretic energy-dissipation capacity by yielding, the reinforcement must be replaced after an earthquake. Furthermore, Ertas and Ozden[3] have demonstrated that as the contribution of mild steel reinforcement to moment capacity increases, the self-centering capacity of the precast, post-tensioned concrete decreases significantly.

Several researchers have developed and tested external dampers to be used in lieu of mild steel in precast, post-tensioned concrete rocking systems with the aim of enhancing energy dissipation capacity with replaceable, reparable, or self-centering devices, thereby reducing seismic displacement demands on the building itself.

Morgen and Kurama[4,5] conducted various subassembly experiments to investigate force-deformation behavior for specimens that had external damping devices designed to work with the principle of translational friction. They concluded that the primary source of energy dissipation in such structures is the dampers and the specimens with dampers could be designed to obtain the minimum energy dissipation ratios prescribed by the American Concrete Institute's *Acceptance Criteria for Moment Frames Based on Structural Testing*, ACI T1.1-01.[6] In contrast, the unbonded, post-tensioned specimens without dampers did not achieve the minimum energy dissipation ratios.

Pampanin et al[7] conducted dynamic shake table tests, using near-field and far-field earthquake records, on precast concrete rocking walls with viscous dampers, metallic yielding dampers, or a combination of both. The investigators concluded that the external devices helped reduce the displacement demands and satisfied the various performance criteria, including limitations on concrete and strand strains. However, the viscous dampers were quite inefficient for low damper-displacement amplitudes. Koshikawa et al.[8,9] carried out parametric analytical studies on the contribution of metallic yielding and friction dampers to the energy dissipation capacity of precast, post-tensioned concrete rocking systems. They concluded that "energy dissipation increases linearly with the increase of both the damper yield force and the distance of the damper from the beam centerline."

Several recent studies have investigated an array of external energy dissipation devices used with precast, post-tensioned concrete rocking systems. These devices included thin rubber layers,[10] steel angles,[11] embedded steel connectors,[12] friction-damped wall joints,[13] replaceable steel bars,[14] and steel plastic hinges[15] that are specially designed to contribute to external energy dissipation.

Theory and explanation of the proposed damper mechanism

Previous research[4–16] on increasing the energy dissipation capacity of precast and post-tensioned concrete rocking systems mostly focused on velocity-dependent (viscous) and displacement-dependent (metallic yielding and translational friction) dampers. The mechanisms for these types of external dampers employ the principles of translational velocity and translational displacement.

The external damper proposed in this research uses the concept of motion amplification, which aims to magnify the seismic displacements and rotations imposed on the joint by the gap-opening mechanism. Although there have been studies of this principle,[17–23] the recent literature has been predominantly focused on toggle brace dampers. Dampers of that type occupy considerable space in buildings and therefore may not be favorable options when compactness is of concern. The proposed damper, which is placed only at a beam-column joint, works with the rotational friction mechanism that occurs on special friction surfaces between the joints of steel plates. Damper systems working with principle of rotational friction have been proposed previously.[24–26] However, those systems are lacking in two fundamental ways. First, because the initial angles of the test systems were not less than 30 degrees, the systems could not take advantage of the motion amplification concept. Second, the friction mechanism in the existing systems occurred only at the middle joint for these dampers; thus, the systems did not take advantage of the relative rotation of the end joints. **Figure 1** shows how a cantilever beam displaced vertically at its end is affected by the proposed mechanism as well as the previously proposed translational friction[4] and metallic yielding[5] mechanisms. In the proposed external damper, as the initial angle of the damper position gets smaller, the relative rotation between surfaces is amplified. Since energy dissipation is directly related to the amount of relative rotation made by these surfaces, this damper design yields an effective external damper device whose damping capacity can be adjusted depending on the demand. To illustrate the motion ampli-

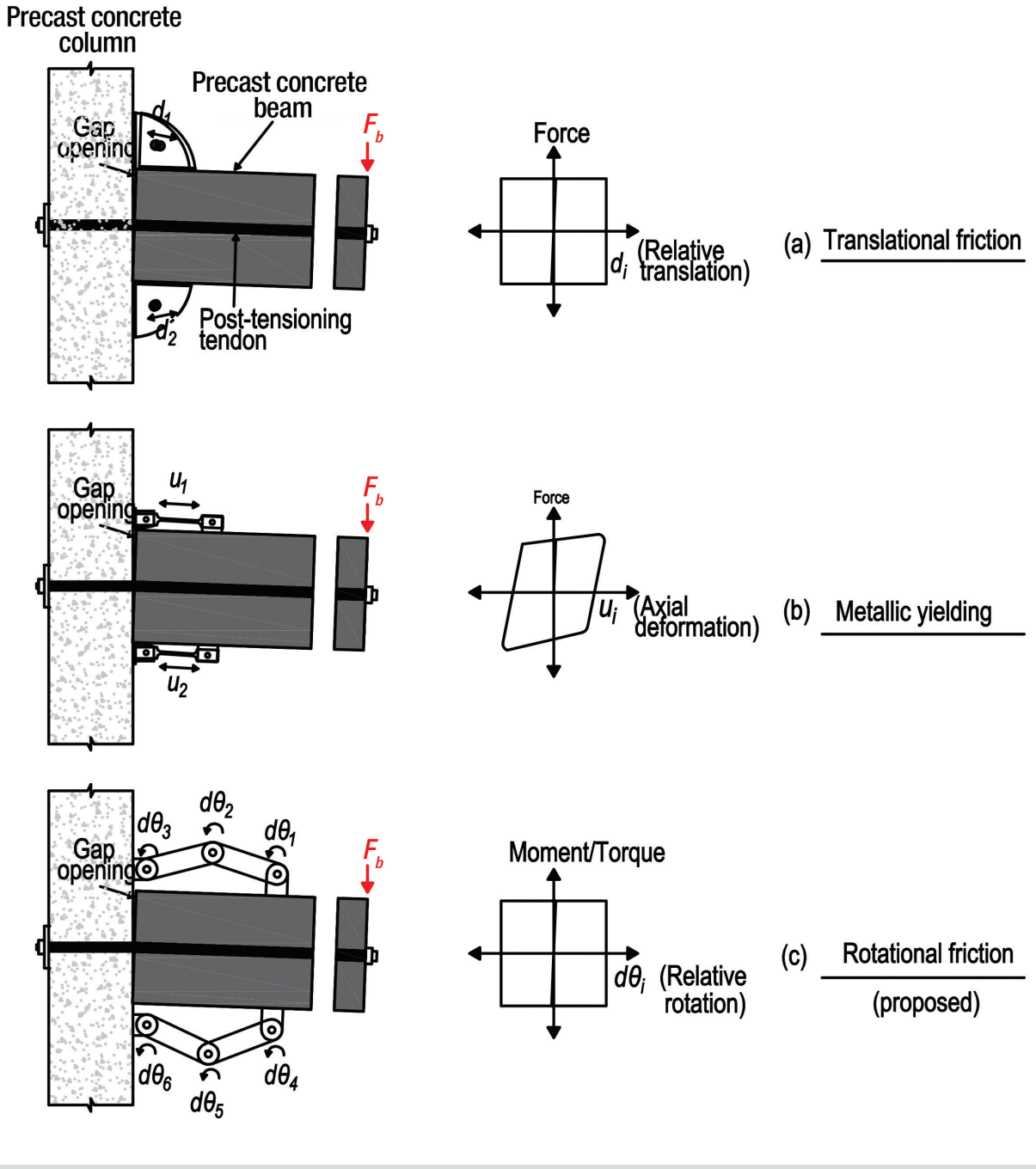

Figure 1. Comparison of translational friction mechanism, metallic yielding mechanism, and proposed (rotational friction) mechanism with amplified damping. Note: d = relative translational displacement; d_i = relative translational displacement at damper component i; $d\theta_1$ = relative rotation at damper joint 1; $d\theta_2$ = relative rotation at damper joint 2; $d\theta_3$ = relative rotation at damper joint 3; $d\theta_4$ = relative rotation at damper joint 4; $d\theta_5$ = relative rotation at damper joint 5; $d\theta_6$ = relative rotation at damper joint 6.; d_1 = relative translational displacement at damper component 1; d_2 = relative translational displacement at damper component 2; F_b = force acting on beam end; u_i = axial deformation of yielding damper component i; u_1 = axial deformation of yielding damper component 1; u_2 = axial deformation of yielding damper component 2.

fication effect of the initial angle, the graph in **Fig. 2** plots data from a kinematic analysis of the proposed damper that takes into account joint rotation. In order to prevent the damper from approaching toggle position during the earthquake and locking itself, it is crucial to determine the initial angle at which the damper enters this position at the maximum expected joint rotation. Consequently, a larger initial angle should be chosen for design to prevent this phenomenon. Kinematics of the damper system is described further in a later section of this article.

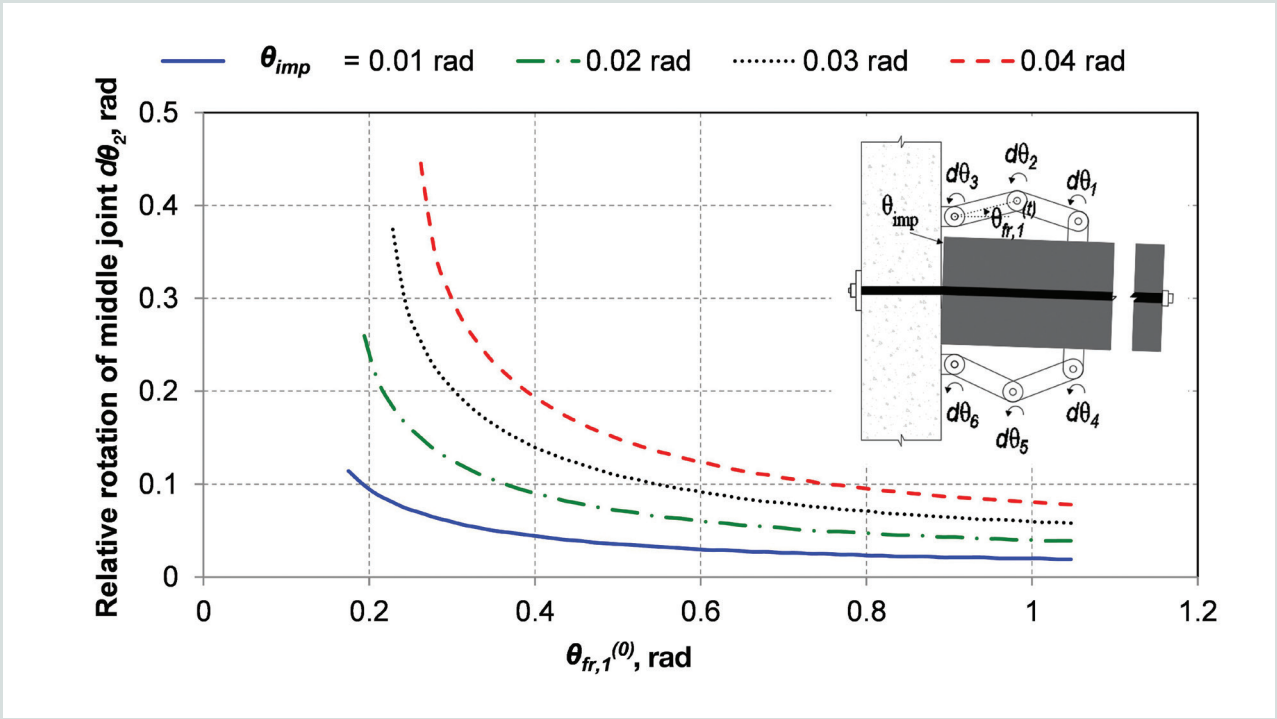

Figure 2. Motion amplification effect of the damper. Note: $\theta_{fr,1}^{(t)}$ = initial angle of the damper at time t; $\theta_{fr,1}^{(0)}$ = initial angle of the damper at time 0; θ_{imp} = imposed rotation at the precast concrete beam-column joint; $d\theta_1$ = relative rotation at damper joint 1; $d\theta_2$ = relative rotation at damper joint 2; $d\theta_3$ = relative rotation at damper joint 3; $d\theta_4$ = relative rotation at damper joint 4; $d\theta_5$ = relative rotation at damper joint 5; $d\theta_6$ = relative rotation at damper joint 6.

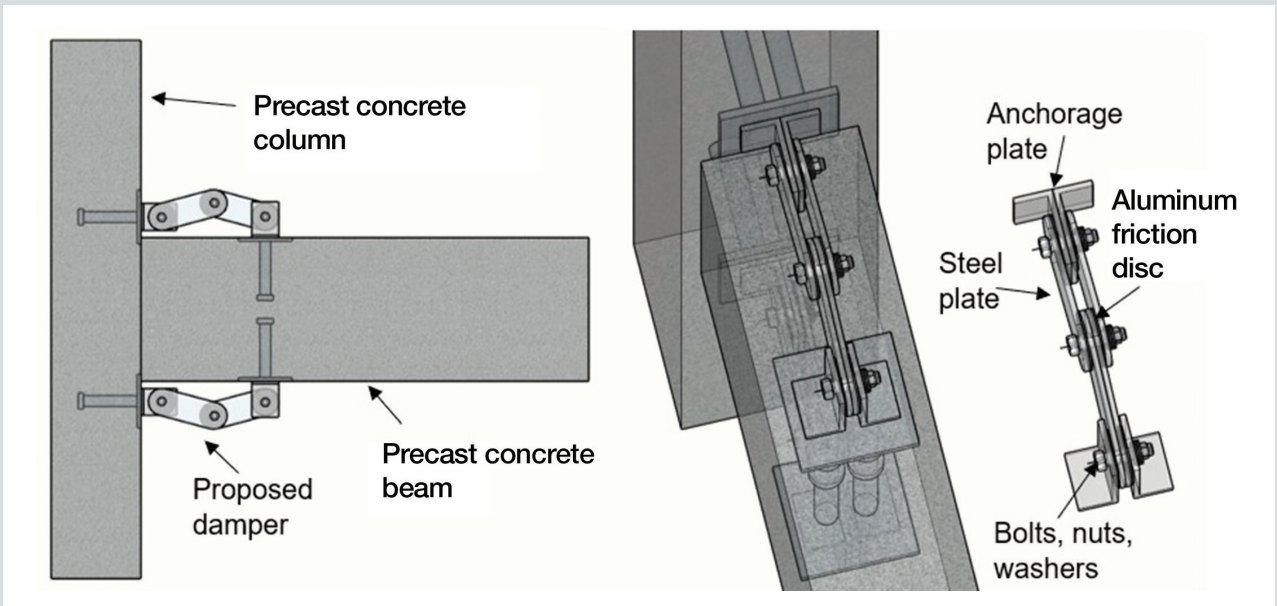

Figure 3. Three-dimensional rendering of the proposed damper mechanism installed on a precast concrete beam-column joint.

Figure 3 presents a three-dimensional rendering of the proposed damper system. The main elements in the damper assembly are the steel plates, steel anchorage members, and aluminum friction discs that are placed in plate-plate and plate–anchorage member connections. The system can be assembled at the construction site following erection of precast concrete components. The necessary clamping force for rotational friction resistance is obtained by using a torque wrench to apply predetermined torques to the bolts.

Numerical model of the proposed damper mechanism

An OpenSees (Open System for Earthquake Engineering Simulation) model of the proposed mechanism was created (**Fig. 4**). Responses predicted with this numerical model were compared with experimental results. For symmetric loading in the experiments, two identical dampers were placed symmetrically with respect to the vertical axis. The part of the model that governed the behavior was the zero-length rotational spring defined at the joints. Two separate nodes with identical coordinates were defined at these joints, and the nodes were kinematically constrained to each other at the x and y directions. For rotation about the z axis, a zero-length rotational spring with a defined nonlinear moment-rotation relationship was assigned between the two nodes. This elastic, perfectly plastic moment-rotation relationship was strictly dependent on the T_{fr} parameter, which is the moment (torque) at which the joint starts relative rotation. This parameter is defined by Eq. (1).

$$T_{fr} = \tfrac{2}{3} n\mu\pi p(r_2^3 - r_1^3) \quad (1)$$

where

n = number of friction surfaces

μ = coefficient of friction between surfaces

p = stress acting on the friction surface due to bolt torque

r_2 = outer radius of the friction surface

r_1 = inner radius of the friction surface

$$p = \frac{N_b}{\pi\left(r_2^2 - r_1^2\right)/2}$$

where

N_b = clamping force acting on the bolt due to applied torque

$$N_b = \frac{T_{blt}}{Kd_{blt}}$$

where

T_{blt} = bolt torque

K = constant for the bolt material and size

d_{blt} = diameter of the bolt

The values of the variables used in this study are: $n = 2$, $r_1 = 15$ mm, $r_2 = 75$ mm, $K = 0.2$ mm, and $d_{blt} = 30$ mm.

Experimental studies of the proposed damper mechanism

Experiments were conducted on the damper mechanism by means of a servo-hydraulic test system, with the test parameters of initial angle $\theta_{fr;1}^{(0)}$, bolt torque in the middle

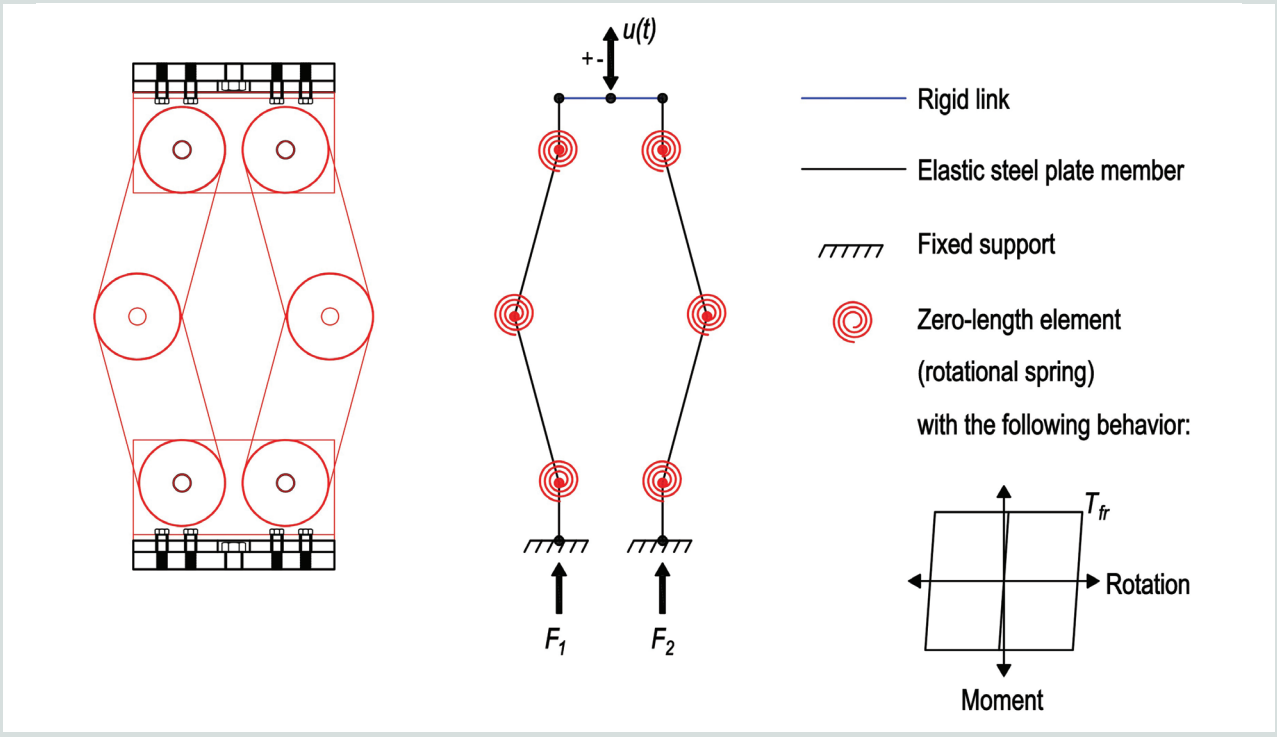

Figure 4. Numerical modeling principles. Note: F_1 = vertical force at the left component of the damper; F_2 = vertical force at the right component of the damper; T_{fr} = frictional clamping torque value applied to the surface of all damper joints for subassembly analyses; $u(t)$ = vertical displacement imposed at the top joint of damper at time t.

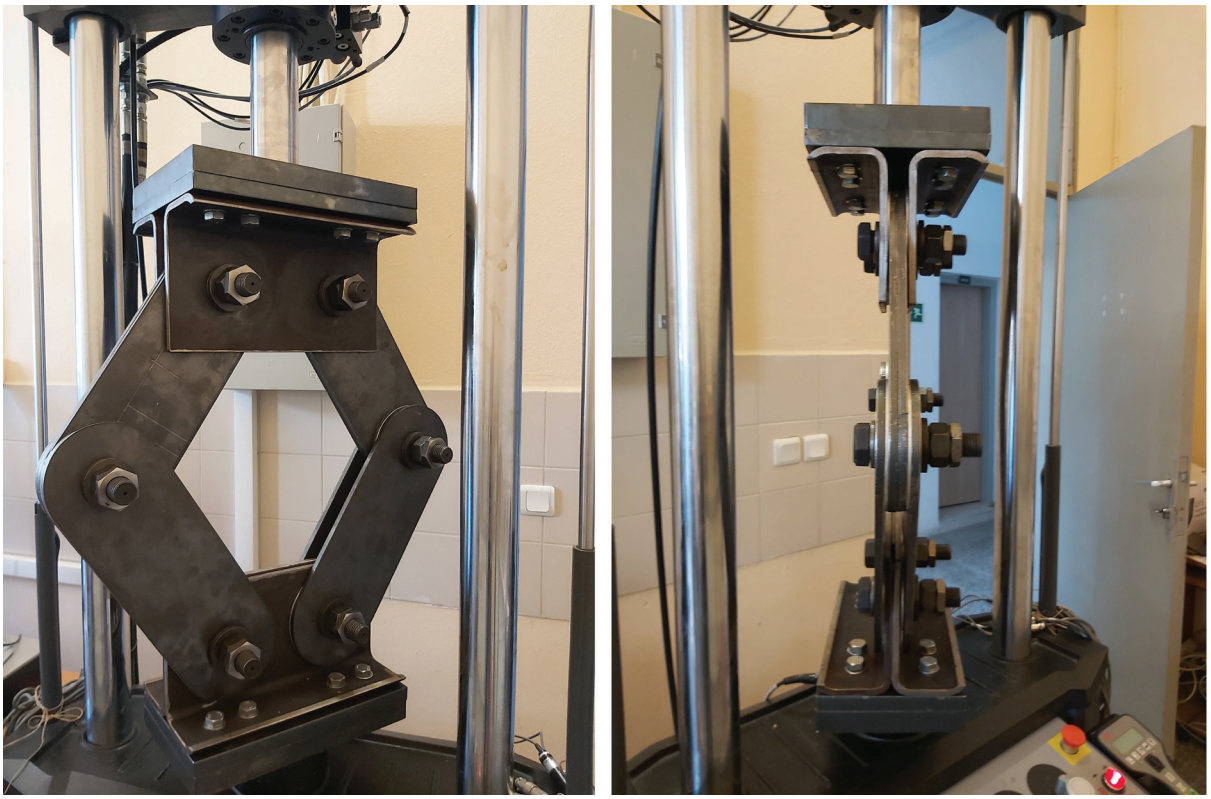

Figure 5. Damper assembly test setup.

joint $T_{blt,m}$, bolt torque in the top and bottom joints $T_{blt,tb}$, and displacement amplitude u_{max}. Since the test system was able to apply the displacement-based protocol in a vertical manner, the damper device was placed accordingly. Furthermore, to prevent the application of any twisting or moment to the test machine, two identical mechanisms were placed symmetrically with respect to the vertical axis. **Figure 5** shows the damper mechanism on the test machine and **Fig. 6** illustrates the damper mechanism's dimensions.

The prototype damper mechanism consisted of four steel plates (two at the top unit, two at the bottom unit) connected to one another at the middle joint and to the anchorage plates at the top and the bottom joints. The damper plates were plasma cut from ST37 Grade steel with specified strength properties of yield strength of structural steel f_{ys} of 300 MPa (43.5 ksi), tensile strength of structural steel f_{us} of 370 MPa (53.6 ksi), and modulus of elasticity of structural steel E_s of 200 GPa (29,000 ksi). The aluminum friction discs were laser cut from 6061 aluminum alloy with specified strength properties of yield strength of aluminum f_{ya} of 275 MPa (39.9 ksi), tensile strength of aluminum f_{ua} of 310 MPa (45.0 ksi), and modulus of elasticity of aluminum E_a of 68 GPa (9860 ksi). The M30 (30 mm [1.2 in.] diameter) bolts and nuts were Grade 8.8 steel (yield strength of bolt f_{yb} of 640 MPa [93 ksi], tensile strength of bolt f_{ub} of 800 MPa [116 ksi], and modulus of elasticity of bolt E_b of 200 GPa [29,000 ksi]). At the end of each bolt, three disc springs, one nut, and one counter-nut were placed. The bolt clamping force was applied using a torque wrench, while the applied torque for each joint was monitored in each test. The damper mechanism was connected to the test machine using steel plates and M16 (16 mm [0.6 in.] diameter) Grade 8.8 steel connection bolts.

Several tests were conducted using the values for control parameters (**Table 1**). The experiments were conducted in accordance with Section 9.3.8 of the Federal Emergency

Table 1. Parameter values in the experiments

Parameter	$\theta_{fr,1}^{(o)}$, deg	$T_{blt,m}$, N-m	$T_{blt,tb}$, N-m	u_{max}, mm
Values	30, 22.5, 15	25, 50, 100	0, 25, 50, 100	5, 15, 25

Note: $T_{blt,m}$ = bolt torque applied to the middle joint in experiments; $T_{blt,tb}$ = bolt torque applied to the top and bottom joints in experiments; u_{max} = maximum vertical displacement amplitude imposed on the damper; $\theta_{fr,1}^{(o)}$ = initial angle of the damper at time 0. 1 mm = 0.0394 in.; 1 N-m = 0.7336 lb-ft.

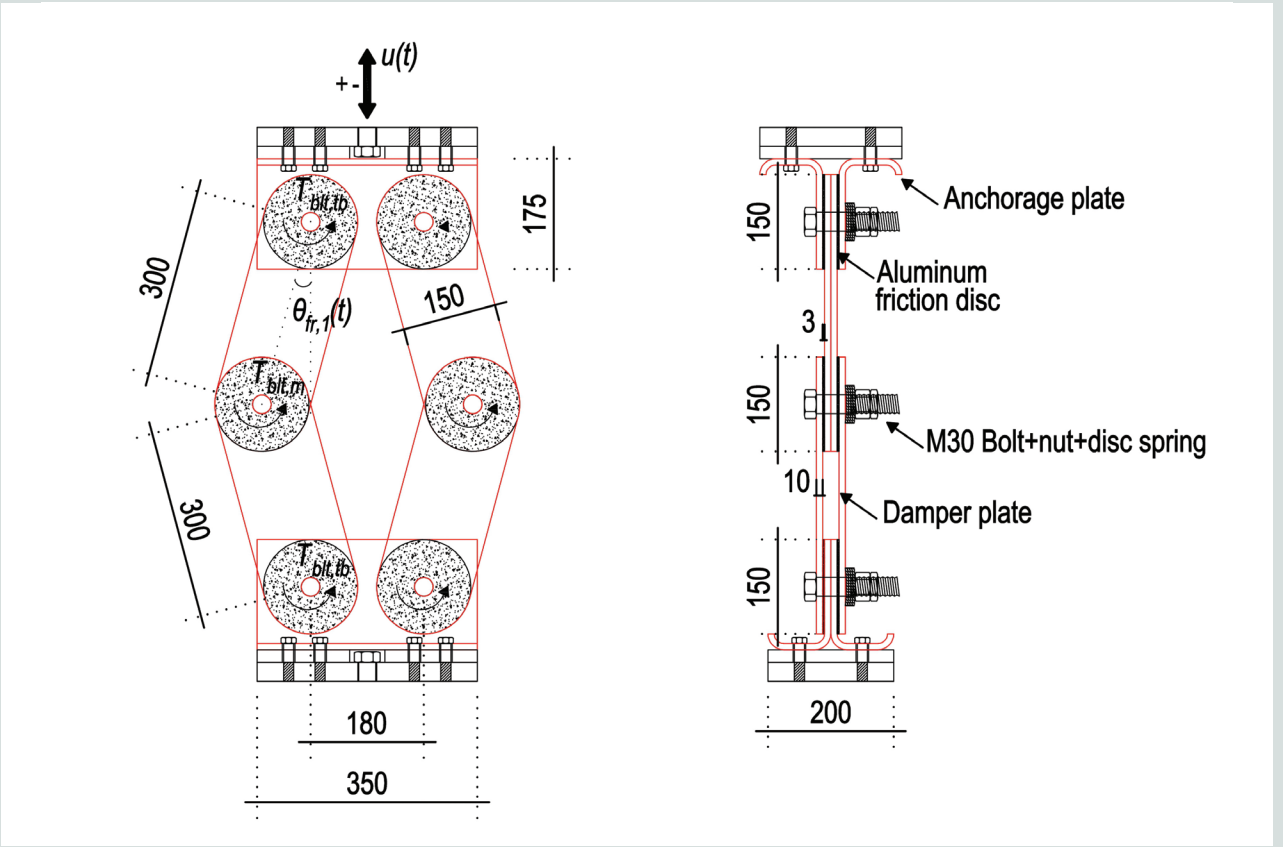

Figure 6. Damper assembly dimensions and parameters. Note: All dimensions are in millimeters. $T_{blt,m}$ = bolt torque applied to the middle joint in experiments; $T_{blt,tb}$ = bolt torque applied to the top and bottom joints in experiments; $u(t)$ = Vertical displacement imposed at the top joint of damper at time t. 1 mm = 0.0394 in.

Management Agency's *Prestandard and Commentary for the Seismic Rehabilitation of Buildings*, FEMA-356.[27] In each experiment, the prototype mechanism was subjected to 30 cycles of loading. Initial angles smaller than 15 degrees were not tested because the mechanism could come close to the toggle position during the tension phase and could lock during the next compression phase in cyclic loading. The experimental results were evaluated in terms of maximum force capacity F_{max} and average value for the area enclosed by force-displacement response $W_{D,avg}$.

Summary of the experimental results

Figure 7 plots the effects of initial angle on force capacity F_{max} and average work done by the closed loop $W_{D,avg}$, along with the force-displacement relationships for tests with $T_{blt,m} = T_{blt,tb}$ = 100 N-m (74 lb-ft). The results demonstrate that as the initial angle $\theta_{fr,1}^{(0)}$ decreased, force capacity and the dissipated energy of the damper increased significantly, particularly when applied bolt torques were larger. Reducing $\theta_{fr,1}^{(0)}$ from 30 to 15 degrees for the dampers with $T_{blt,m} = T_{blt,tb}$ = 100 N-m increased F_{max} from 22 kN (5 kip) to 65 kN (15 kip), whereas that reduction in $\theta_{fr,1}^{(0)}$ more than doubled the work done by the closed loop $W_{D,avg}$. This phenomenon can also be observed in the force-displacement plots (Fig. 7).

For the test with an initial angle of 15 degrees, the behavior became asymmetric as the force capacity of the damper exponentially increased and the displacement amplitude was increased. The relationship between the initial angle and the area under the closed loop is also visible in the force-displacement plots.

Experimental validation of the numerical model

The coefficient of friction μ value of the friction surfaces in Eq. (1) for T_{fr} was determined by using the experiment results to calibrate the numerical model. A mean value of 0.39 for μ satisfied the correlation between numerical and experimental results. This value is close to the coefficient of friction value of 0.40 given for aluminum-steel surfaces in the literature.[28] Frictional clamping torque T_{fr} values corresponding to a T_{blt} of 25, 50, and 100 N-m (18, 37, and 74 lb-ft) as per Eq. (1) were 0.34, 0.68, and 1.36 kN-m (0.25, 0.50, and 1.00 kip-ft), respectively. **Figure 8** presents force-displacement plots comparing experimental test results with results from the numerical model. Comparison of these plots illustrates that the numerical modeling principles outlined previously accurately captured the experimental behavior.

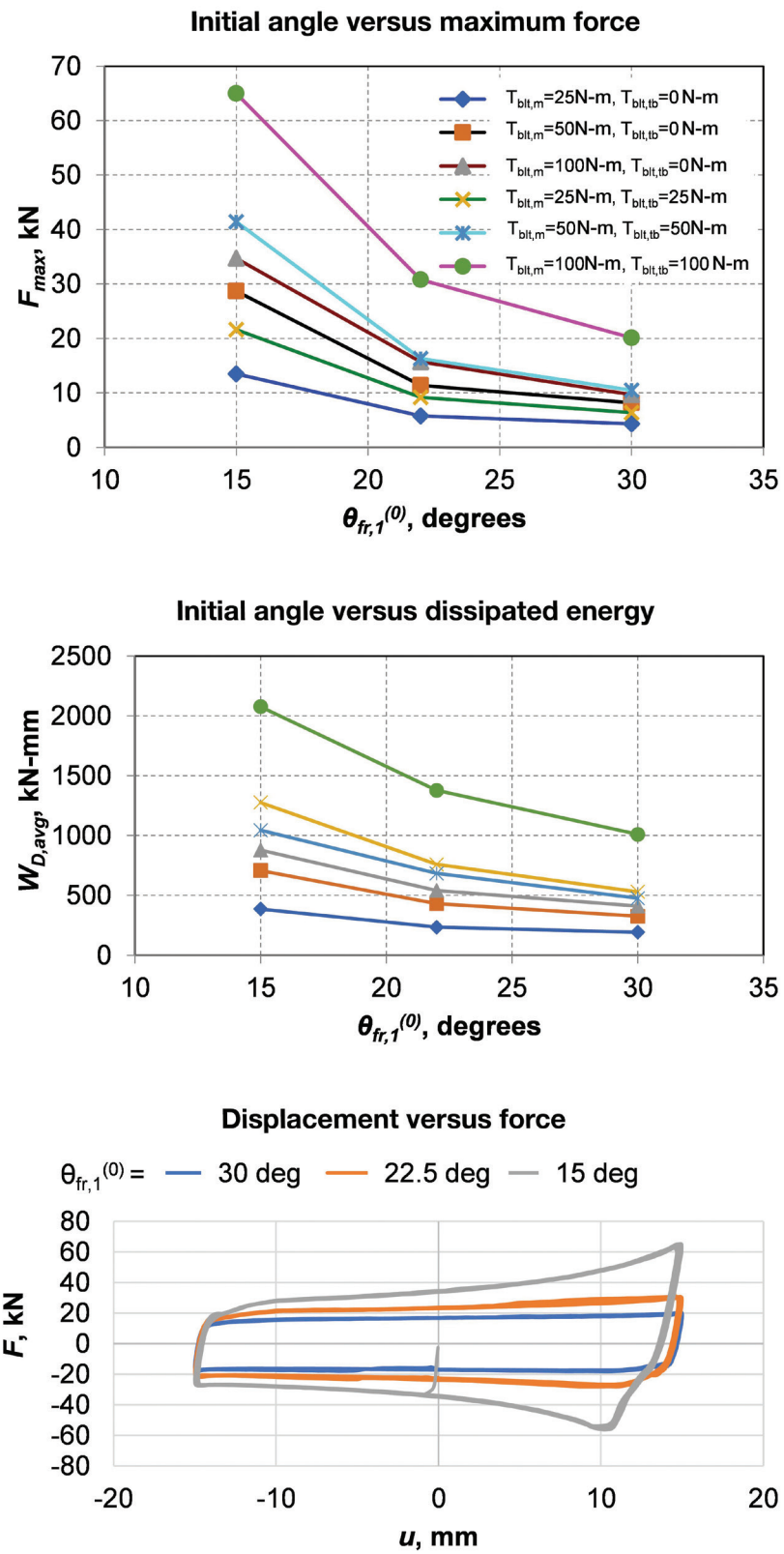

Figure 7. Experimental results. Note: F = Total vertical force acting on the damper; F_{max} = maximum force capacity of the test specimen; $T_{blt,m}$ = bolt torque applied to the middle joint in experiments; $T_{blt,tb}$ = bolt torque applied to the top and bottom joints in experiments; u = vertical displacement imposed on the damper; $W_{D,avg}$ = average area of hysteresis loop for all cycles; $\theta_{fr,1}^{(0)}$ = initial angle of the damper at time 0. 1 mm = 0.0394 in.; 1 kN = 0.225 kip; 1 N-m = 0.7376 lb-ft; 1 kN-mm = 8.851 lb-in.

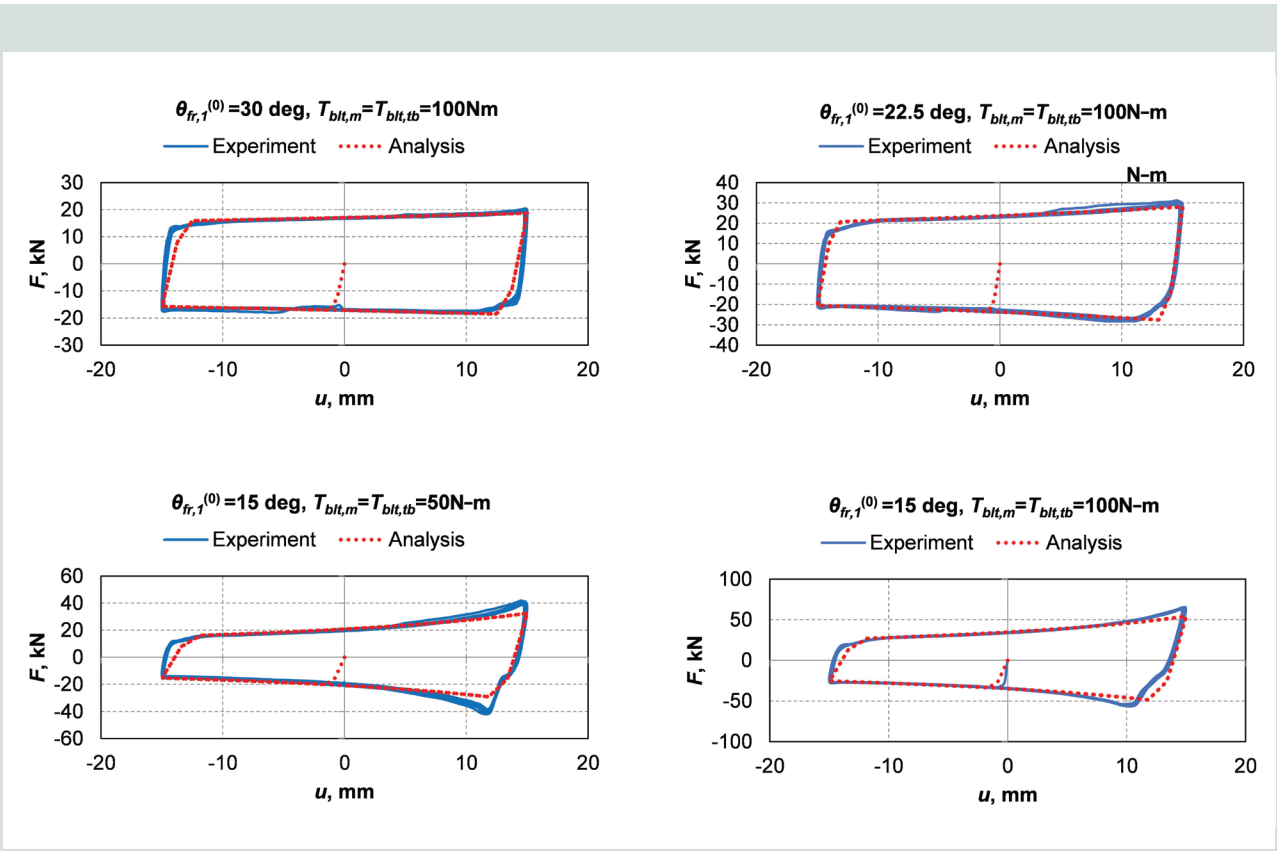

Figure 8. Comparison of numerical analysis and experimental results. Note: F = Total vertical force acting on the damper; $T_{blt,m}$ = bolt torque applied to the middle joint in experiments; $T_{blt,tb}$ = bolt torque applied to the top and bottom joints in experiments; u = Vertical displacement imposed on the damper; $\theta_{fr,1}^{(0)}$ = initial angle of the damper at time 0. 1 mm = 0.0394 in.; 1 kN = 0.225 kip; 1 N-m = 0.7376 lb-ft.

Numerical studies

To investigate the behavior of precast, post-tensioned concrete rocking systems with the proposed dampers, a representative frame and 10 subassemblies to obtain the cyclic force-displacement response were analyzed. **Figure 9** shows the representative frame and **Fig. 10** shows details for the subassembly analyses. The damper parameters (dimensions and bolt torques) were designed according to the performance demands of the frame-level analyses. Given the limited force capacity of the testing equipment, the damper parameters in the experiments were scaled down. This scaling was done by using Eq. (1) to obtain maximum bolt torque that can be applied without exceeding the vertical force capacity of the testing equipment. Numerical modeling of the damper (Fig. 4) was used to relate the capacity of the testing machine to the friction torques calculated by Eq. (1). In the numerical analyses, a larger-size damper mechanism was used (Fig. 10).

The principles described by Morgen and Kurama[4] were used to model the subassemblies and the frames in the OpenSees finite element model. The precast concrete beam and column elements were modeled using two-dimensional, displacement-based beam-column elements (*dispBeamColumn*) in OpenSees. These elements incorporate fiber sections with *Concrete02* material as concrete and *Steel01* material as reinforcement bars. A short (20 mm [0.8 in.]), nonlinear beam element with no tensile stiffness in concrete fibers (*Concrete01*) and no reinforcement bars was defined to account for the unique gap-opening behavior at the joint interface. The unbonded post-tensioning tendons were modeled using truss elements. The initial jacking stresses were defined by *InitStressMaterial*, which was then assigned to *ElasticMultiLinear* material used in the truss elements. The initial jacking stress of tendons was half the ultimate strength. The anchorage of post-tensioning tendons to beam ends was modeled using rigid links that kinematically constrain relevant nodes. In Fig. 9 and 10, post-tensioning tendons are shown as vertically offset from beams for the sake of illustration. In the numerical model, the tendons were kinematically constrained to beam end nodes with identical coordinates. The damper mechanisms were also kinematically constrained by rigid links to the corresponding nodes at beam and column elements.

This research verified the numerical modeling principles outlined herein by comparing the analysis results with the experimental results of Ertas and Ozden[3] at the subassembly level and the parametric results of Morgen and Kurama[5] at the frame level.

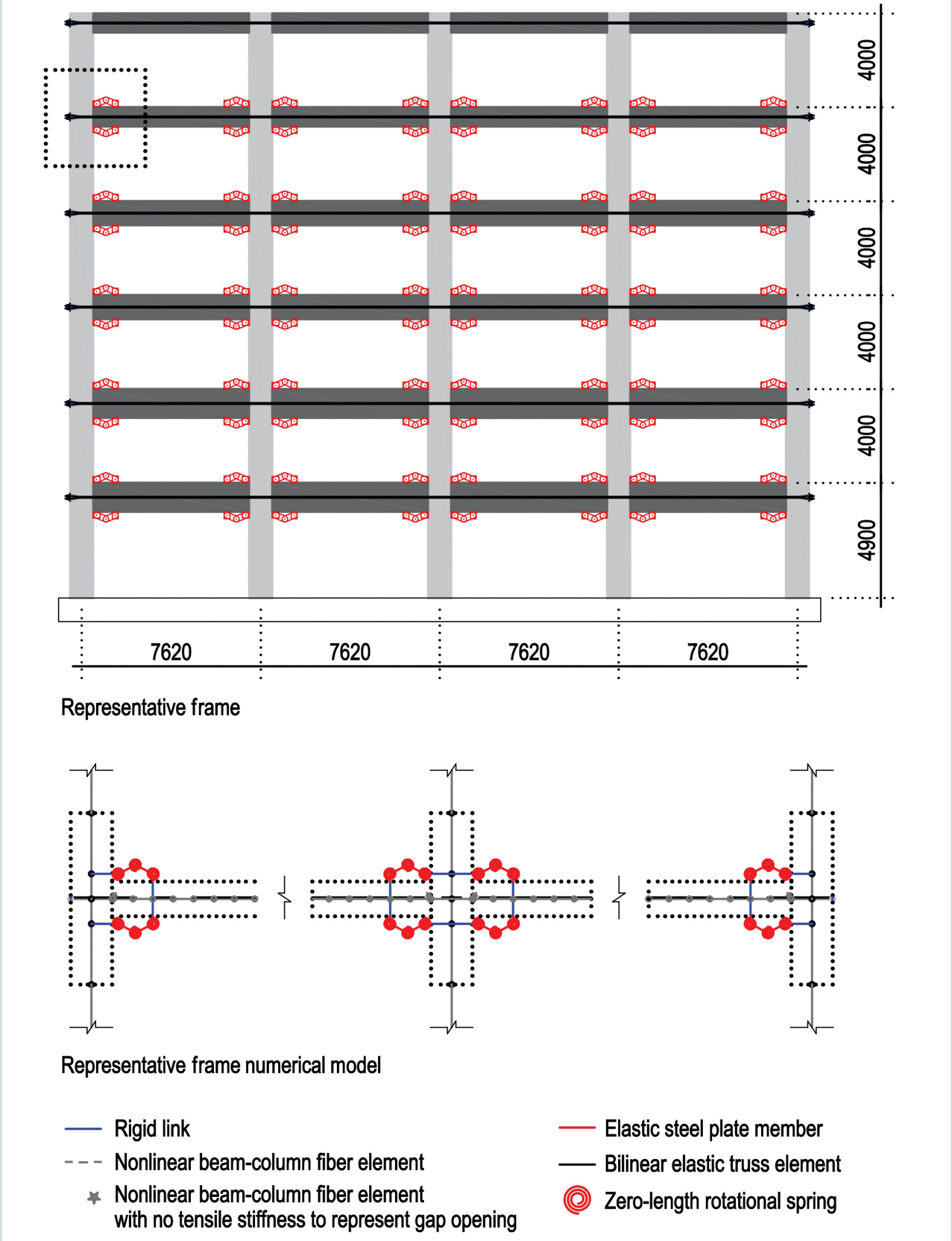

Figure 9. Representative frame and representative frame numerical model in OpenSees. Note: All dimensions are in millimeters. OpenSees = Open System for Earthquake Engineering Simulation. 1 mm = 0.0394 in.

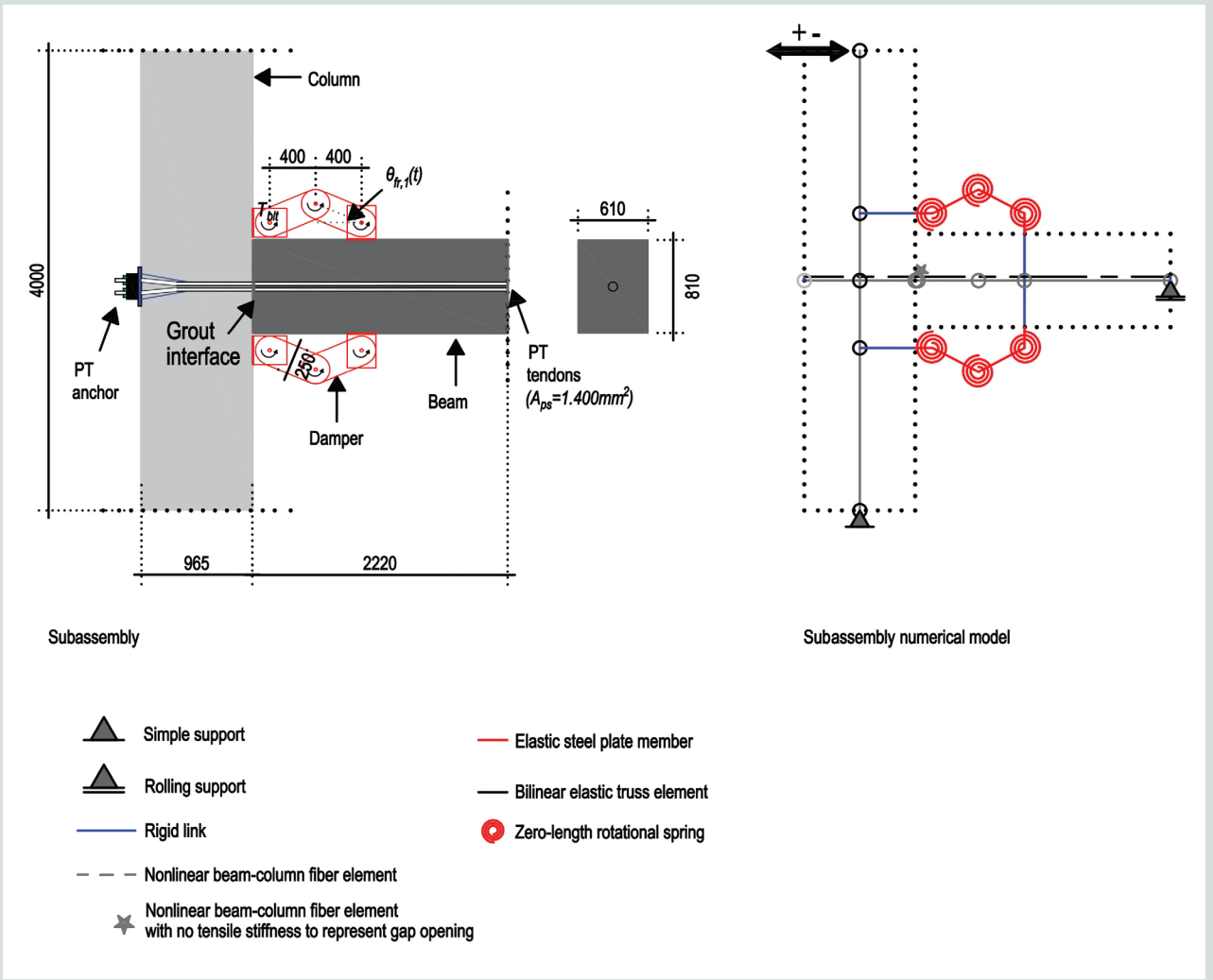

Figure 10. Subassembly and subassembly numerical model in OpenSees. Note: All dimensions are in millimeters. A_{ps} = total cross-sectional area of one layer of post-tensioning strands; OpenSees = Open System for Earthquake Engineering Simulation; PT = post-tensioned; T_{blt} = bolt torque; $\theta_{fr,1}^{(t)}$ = initial angle of the damper at time t. 1 mm = 0.0394 in; 1 mm² = 0.00155 in.²

Subassembly-level analyses

The numerical modeling principles were used to analyze the effect of the initial angle $\theta_{fr,1}^{(0)}$ and bolt torque T_{blt} on the response of the subassemblies. Equal bolt torques were applied to all damper joints in the model. The energy dissipation capacity of systems is quantified in ACI T1.1-01[6] by the relative energy dissipation ratio β, which is defined as

> *the ratio of actual to ideal energy dissipated by test module during reversed cyclic response between given drift ratio limits, expressed as the ratio of the area of the hysteresis loop for that cycle to the area of the circumscribing parallelograms defined by the initial stiffness during the first cycle and the peak resistance during the cycle for which the energy dissipation ratio is calculated.*

This parameter is formulated by the following relation and is deemed insufficient if its value is less than 0.125 for third cycle of drift ratio of 3.50%:

$$\beta = \frac{A_h}{(E_1 + E_2)(\theta_1' + \theta_2')}$$

where

A_h = total area of the hysteresis loop

E_1 = peak lateral resistance for positive loading for the relevant sequence

E_2 = peak lateral resistance for negative loading for the relevant sequence

θ_1' = drift ratio for zero lateral load for unloading at initial stiffness from peak positive resistance

θ_2' = drift ratio for zero lateral load for unloading at initial stiffness from peak negative resistance

In accordance with the acceptance criteria from ACI T1.1-01,[6] the top nodes of the columns for subassemblies with varying parameters were subjected to a displacement protocol corresponding to ±0.15%, ±0.20%, ±0.25%, ±0.35%, ±0.50%, ±0.75%, ±1.00%, ±1.40%, ±1.75%, ±2.20%, ±2.75%, ±3.50%, and ±4.00% relative drifts. **Table 2** shows the parameters of the 10 subassemblies (SU0–SU09) along with relative energy dissipation ratio β values obtained from OpenSees cyclic hysteresis results for the selected drift ratios. **Table 3** presents initial stiffness values K_i along with force capacities F_r with respect to drift demands. **Figure 11** shows cyclic hysteresis curves for the subassemblies.

SU0 was the baseline subassembly with no damper. SU1 was the baseline subassembly with the addition of parameters to constitute a reference to observe the effect of the initial damper angle. SU2 through SU5 were subassemblies with decreasing initial damper angles and SU6 through SU9 were

Table 2. Relative energy dissipation ratios for subassemblies analyzed in OpenSees

SU	$\theta_{fr,1}^{(o)}$, deg	T_{blt}, N-m	T_{fr}, kN-m	β							
				±0.50%	±0.75%	±1.40%	±1.75%	±2.20%	±3.50%	±4.00%	Average
0	22.50	0	0	0.008	0.009	0.013	0.010	0.011	0.013	0.010	0.010
1	22.50	444	10	0.170	0.183	0.183	0.178	0.172	0.164	0.161	0.152
2	30.00	444	10	0.120	0.136	0.140	0.136	0.131	0.124	0.121	0.109
3	26.25	444	10	0.142	0.157	0.159	0.154	0.149	0.141	0.138	0.128
4	18.75	444	10	0.206	0.218	0.216	0.210	0.204	0.196	0.195	0.185
5	15.00	444	10	0.255	0.265	0.261	0.256	0.251	0.239	0.231	0.231
6	15.00	89	2	0.073	0.076	0.077	0.073	0.073	0.077	0.078	0.071
7	15.00	267	6	0.178	0.184	0.181	0.177	0.175	0.173	0.171	0.164
8	15.00	623	14	0.313	0.328	0.324	0.318	0.310	0.287	0.272	0.280
9	15.00	801	18	0.356	0.376	0.374	0.367	0.357	0.325	0.304	0.316

Note: OpenSees = Open System for Earthquake Engineering Simulation; SU = subassembly; T_{blt} = bolt torque; T_{fr} = frictional clamping torque value applied to the surface of all damper joints for subassembly; β = relative energy dissipation ratio; $\theta_{fr,1}^{(o)}$ = initial angle of the damper at time 0. 1 kN/m = 0.069 kip/ft; 1 N-m = 0.7376 lb-ft; 1 kN-m = 0.7376 kip-ft.

Table 3. Force capacities and initial stiffness values for sub-assemblies analyzed in OpenSees

SU	$\theta_{fr,1}^{(o)}$, deg	T_{blt}, N-m	T_{fr}, kN-m	F_r, kN							K_i, kN/m
				±0.50%	±0.75%	±1.40%	±1.75%	±2.20%	±3.50%	±4.00%	
0	22.50	0	0	179	190	218	233	251	287	292	616,000
1	22.50	444	10	223	235	264	281	301	342	349	642,000
2	30.00	444	10	212	224	252	268	287	324	329	631,000
3	26.25	444	10	217	229	257	273	292	331	337	636,000
4	18.75	444	10	231	244	275	293	314	364	376	652,000
5	15.00	444	10	244	259	296	317	346	444	502	667,000
6	15.00	89	2	191	203	232	249	269	317	333	628,000
7	15.00	267	6	217	230	264	282	307	380	418	650,000
8	15.00	623	14	272	288	328	353	385	506	583	682,000
9	15.00	801	18	300	317	361	389	426	568	660	694,000

Note: F_r = maximum force capacity of the subassembly at the given drift ratio; K_i = initial stiffness; OpenSees = Open System for Earthquake Engineering Simulation; SU = subassembly T_{blt} = bolt torque; T_{fr} = frictional clamping torque value applied to the surface of all damper joints for subassembly; $\theta_{fr,1}^{(o)}$ = initial angle of the damper at time 0. 1 kN/m = 0.069 kip/ft; 1 N-m = 0.7376 lb-ft; 1kN-m = 0.7376 kip-ft.

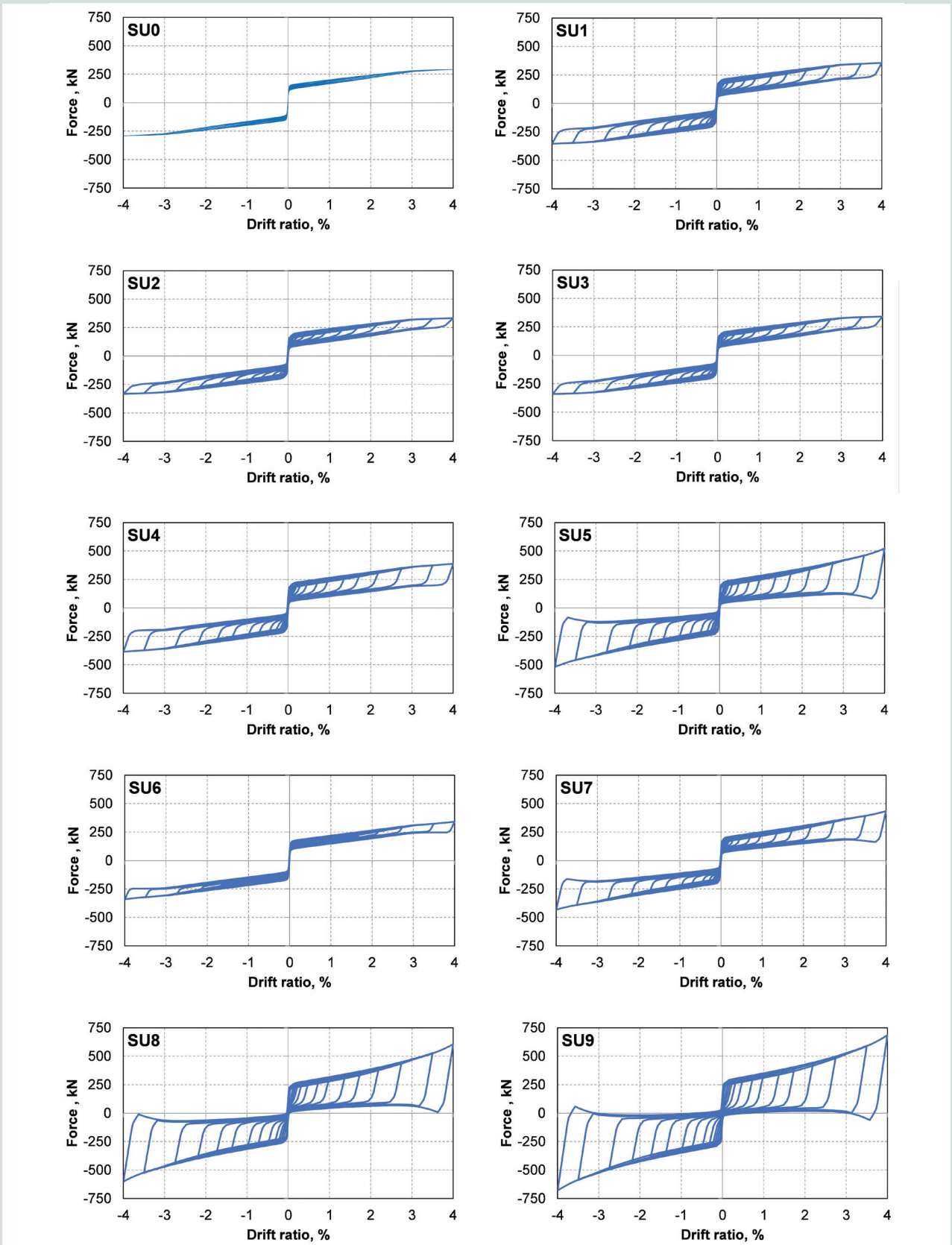

Figure 11. Force versus drift-ratio relationships for the subassemblies. Note: SU0 = subassembly 0; SU1 = subassembly 1; SU2 = subassembly 2; SU3 = subassembly 3; SU4 = subassembly 4; SU5 = subassembly 5; SU6 = subassembly 6; SU7 = subassembly 7; SU8 = subassembly 8; SU9 = subassembly 9. 1 kN = 0.225 kip.

subassemblies subjected to increasing bolt torques for the case where $\theta_{fr,1}^{(0)}$ = 15 degrees.

General interpretation of subassembly-level results

SU0, the subassembly without dampers, did not satisfy the minimum ACI T1.1-01[6] requirement of 0.125 for β for any of the drift ratios. This finding demonstrates that an unbonded, post-tensioned, precast concrete rocking system would not have sufficient energy dissipation capacity. All of the other subassemblies except for SU2 and SU6 satisfied the minimum ACI T1.1-01 requirement for all drifts.

The energy dissipation provided by the proposed damper was significant for small drift demands. This finding implies that the amplifying aspect of the damper would be effective for light to moderate seismic effects.

The force capacities of the subassemblies were significantly increased with the dampers, particularly when initial angle $\theta_{fr,1}^{(0)}$ was small. A small initial angle (less than 20 degrees) also prevented stiffness reduction, which otherwise would occur due to the yielding of post-tensioning tendons.

Compared with subassembly SU0, the other subassemblies did not exhibit dramatic increases in initial stiffness, implying that the reduction in seismic drift demands would be primarily due to energy dissipation related to the dampers, rather than stiffening of the structure, which would increase seismic force demands on the system. On the other hand, the dampers had a dramatic effect on moment capacity.

All of the subassemblies demonstrated self-centering capability, mainly by exhibiting very small residual deformations in all drift demands.

Effect of initial damper angle

Figure 12 illustrates the effect of initial damper angle on the relative energy dissipation ratio and force capacity of the subassemblies. Decreasing the initial angle of the damper

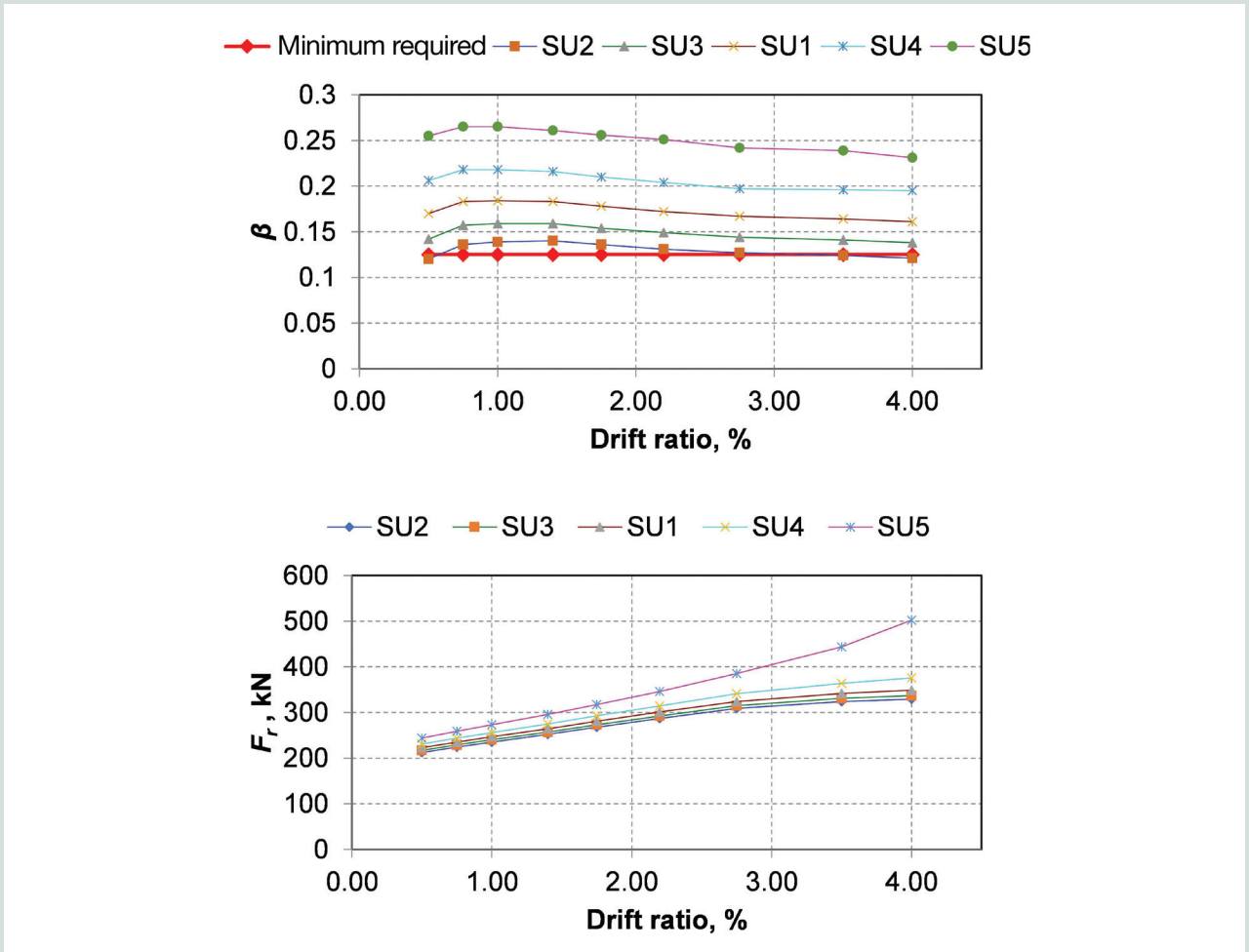

Figure 12. Effect of initial angle on subassembly behavior. Note: F_r = maximum force capacity of the subassembly at the given drift ratio; SU1 = subassembly 1; SU2 = subassembly 2; SU3 = subassembly 3; SU4 = subassembly 4; SU5 = subassembly 5; β = relative energy dissipation ratio. 1 kN = 0.225 kip.

significantly increased the energy dissipation capacity of the system. For example, for 2.20% drift, β was equal to 0.131 for an initial angle of 30 degrees, whereas β increased to 0.251 for an initial angle of 15 degrees. Moreover, the average values of β were 0.109 and 0.231 for 30 degrees and 15 degrees, respectively. These findings demonstrate the amplifying effect of the damper.

Notably, the β value tended to decrease as the drift ratio increased. This finding is explained by the fact that the work done by the closed area under the loop increased less than the parallelogram enclosed by the initial stiffness and force capacity of the subassembly.

Decreasing the initial angle had a dramatic effect on force capacity, particularly for larger drift demands. For 4.00% drift, reducing the initial angle from 30 to 15 degrees increased the force capacity from 329 to 502 kN (74 to 113 kip). The substantial increase in the capacity that was achieved by reducing the initial angle further highlights the novel aspect of the proposed damper.

As the post-tensioning tendons reached the limit of linear proportionality, a softening in stiffness of the system was observed for subassemblies with an initial angle larger than 15 degrees (SU0 through SU4). However, the small initial angle of the damper caused the force contribution of the damper to exponentially increase, thereby compensating for the stiffness and force-capacity loss associated with the yielding of post-tensioning tendons (SU5 through SU9).

Changing the initial angle slightly influenced the initial stiffness of the subassembly. When results for SU2 and SU5 were compared, decreasing the initial angle of the damper increased the stiffness by only 6%. This finding indicates that the damper can be effective in reducing seismic-displacement demands by providing a large amount of energy dissipation rather than by stiffening the structure.

Effect of bolt torque

Figure 13 presents the effect of bolt torque in terms of the relative energy dissipation ratio and force capacity. Increasing

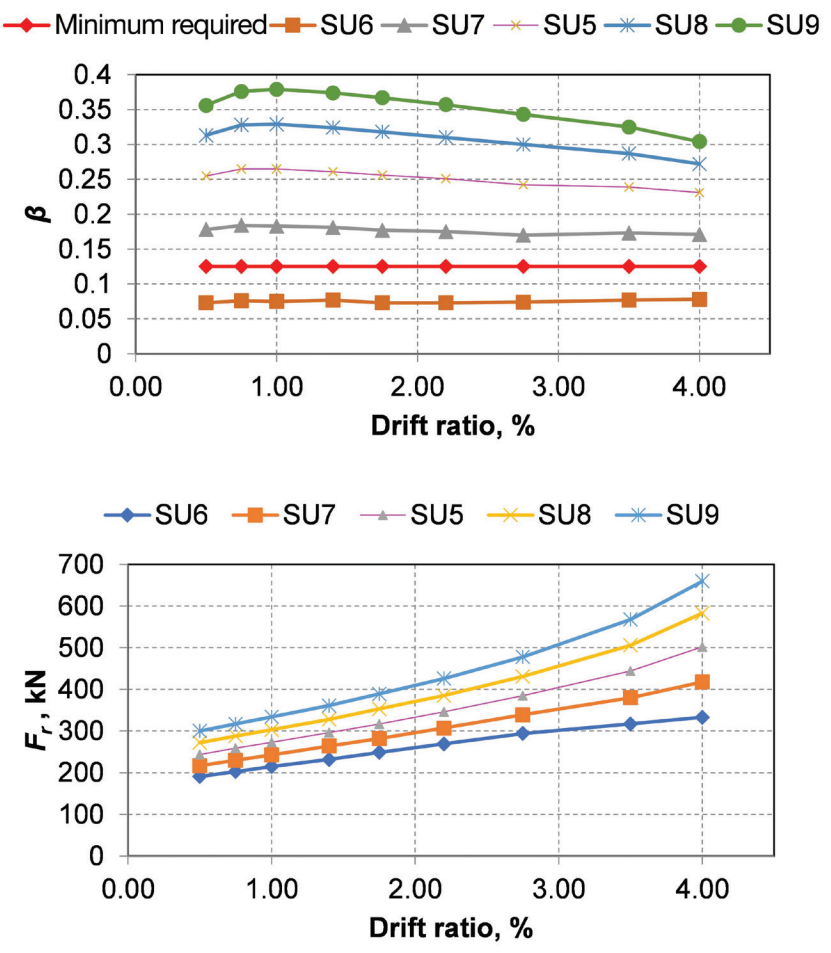

Figure 13. Effect of friction torque on subassembly behavior. Note: F_r = maximum force capacity of the subassembly at the given drift ratio; SU5 = subassembly 5; SU6 = subassembly 6; SU7 = subassembly 7; SU8 = subassembly 8; SU9 = subassembly 9; β = relative energy dissipation ratio. 1 kN = 0.225 kip.

bolt torque increased the energy dissipation. However, there was no linear relationship between bolt torque and energy dissipation. For example, SU9, whose bolt torque was nine times greater than that of SU6, had an average energy dissipation ratio that was roughly five times greater than that of SU6.

For small drift demands, the effect of increasing bolt torque was smaller. Increasing bolt torque had a negligible effect on initial stiffness of the system. In contrast, bolt torque provided a large additional force capacity to the system. However, as was the case with energy dissipation, force capacity was not linearly correlated with bolt torque. This finding is expected because post-tensioning tendons also contribute to force capacity.

Frame-level analysis results

The representative frame (Fig. 9) was analyzed to investigate the effect of dampers on frame behavior and to take into account gravitational loads, which were applied as point loads to beam nodes. Two parametric frames, one without any external dampers and one with the proposed dampers, were analyzed under imposed roof drifts of ±0.50%, ±1.00%, ±2.00% and ±3.50%. The dampers were designed so that the damped frame would have the same base shear capacity as the undamped frame. The initial angle $\theta_{fr,1}^{(0)}$ for the dampers was 15 degrees, whereas the dimensions were chosen to be the same as those in subassembly analyses. **Table 4** presents the parameters for the frames.

Figure 14 shows the drift ratio versus base shear results for the frames and **Table 5** presents the results for the relative energy dissipation ratio β. The damped frame had larger work done inside the closed loop (Fig. 14), which was also shown by the significantly larger relative energy dissipation ratios in Table 5.

The undamped frame did not satisfy the minimum requirement for β, whereas the damped frame satisfied the minimum requirement for β for all drifts. The post-yield stiffness of the damped frame was also greater than that of the undamped frame due to the exponentially increasing effect of damper contribution to force capacity. The increase in post-yield stiffness is because of the small initial angle $\theta_{fr,1}^{(0)}$ chosen for the dampers.

Kinematics of the damper system

To prevent locking of the damper under expected joint rotation demand, it is important to perform kinematic analysis to determine the minimum initial angle $\theta_{fr,1}^{(0)}$ at which the damper does not take a collinear form (toggle position) under this demand. This analysis can be done by imposing the maximum expected rotation θ_{jo} to the joint and applying the principle of closed-loop vectors to the displaced geometry to determine the positions of damper joints.

The relationship of the damper joint locations with respect to the imposed joint rotation θ_{jo} is expressed as follows:

$$\bar{A}\cos\alpha_A + \bar{B}\cos\alpha_B = \bar{C}\cos\alpha_C + \bar{D}\cos\alpha_D$$

$$\bar{A}\sin\alpha_A + \bar{B}\sin\alpha_B = \bar{C}\sin\alpha_C + \bar{D}\sin\alpha_D$$

where

$\bar{A}$ = magnitude of vector A

α_A = angle between vector A and positive x axis

$\bar{B}$ = magnitude of vector B

α_B = angle between vector B and positive x axis

$\bar{C}$ = magnitude of vector C

α_C = angle between vector C and positive x axis

$\bar{D}$ = magnitude of vector D

α_D = angle between vector D and positive x axis

Table 4. Frame parameters

Floor	1	2	3	4	5	6
Member dimensions for both frames, mm						
Columns	710/965					
Beams	610/1220	610/1220	610/1015	610/1015	610/810	610/810
Post-tensioning tendon area A_{ps}, mm²						
Undamped frame	7942	7024	7264	5174	3304	1490
Damped frame	6026	5599	5949	4213	2774	1490
Damper bolt torques T_{blt}, N-m						
Undamped frame	0	0	0	0	0	0
Damped frame	1110	1055	945	775	500	0

Note: 1 mm = 0.0394 in.; 1 mm² = 0.00155 in.²; 1 N-m = 0.7376 lb-ft.

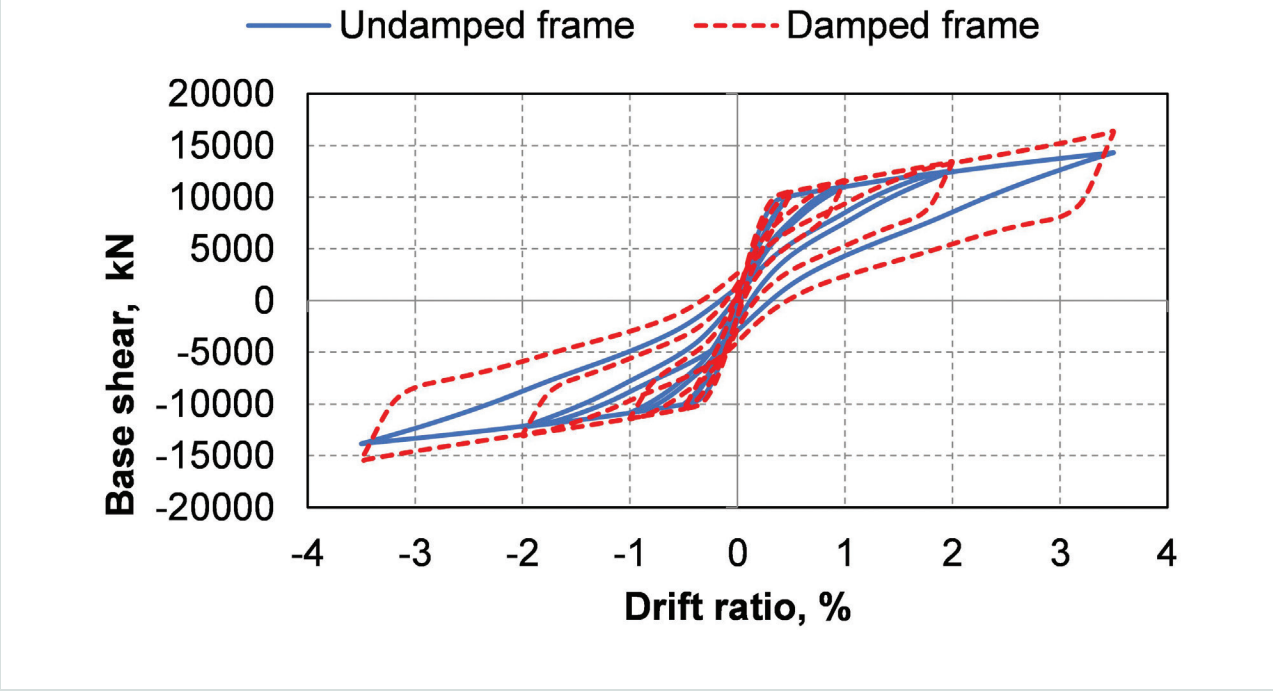

Figure 14. Base shear versus drift ratio plots for frame analyses. Note: 1 kN = 0.225 kip.

The point about which the joint rotates, which has distance c_c away from extreme beam fiber (**Fig. 15**), can be determined iteratively by using section equilibrium. The initial angle at which the damper locks itself under joint rotation demand can be determined by equating α_D to 180 degrees for the rotation direction.

Conclusion

This research proposes a novel external damping system working with principle of rotational friction to limit seismic displacement demands on precast, post-tensioned concrete structures, which have small energy dissipation capacities due to their unique behavior. Experiments were conducted on a prototype damper mechanism to investigate the effect of various parameters on the force-displacement response and to verify the numerical modeling principles. Numerical studies of the subassemblies showed that the proposed damper mechanism increased the energy dissipation and force capacity of unbonded, post-tensioned rocking systems. The geometrical disposition of the damper amplified the displacements imposed by earthquakes, potentially providing a large amount of energy dissipation. The self-centering effect of post-tensioning strands prevents large residual deformations in the system, forcing it to return to its original configuration after an earthquake. The self-centering effect of strands is particularly significant because dampers working with a friction mechanism do not have self-centering capability. However, a balanced design methodology should be followed to ensure that the dampers provide sufficient energy dissipation capacity while the post-tensioning strands remain elastic after the earthquake. It is also imperative to determine the initial angle at which the damper does not lock itself for the expected maximum joint rotation.

Table 5. Relative energy dissipation ratios β for frame analyses

	β			
Frame	**Drift ratio, %**			
	±0.50	±1.00	±2.00	±3.50
Undamped	0.108	0.100	0.116	0.123
Damped	0.225	0.229	0.242	0.250

The numerical studies of a representative frame with and without proposed dampers indicated that the proposed dampers would provide a significant increase in energy dissipation and post-yield stiffness to the structure, reducing the amount of post-tensioning tendons required to withstand seismic forces. Unlike the classical toggle-brace dampers that work with displacement amplification principle, the proposed dampers would not occupy a large space within a building. The proposed dampers are also novel in the sense that previous research involving rotational friction dampers did not use the motion amplification mechanism and did not have contribution from the end joints to the energy dissipation. Additional experimental studies on precast, post-tensioned concrete beam-column subassemblies incorporating the proposed dampers would help researchers better understand the behavior of precast, post-tensioned concrete rocking systems with these dampers.

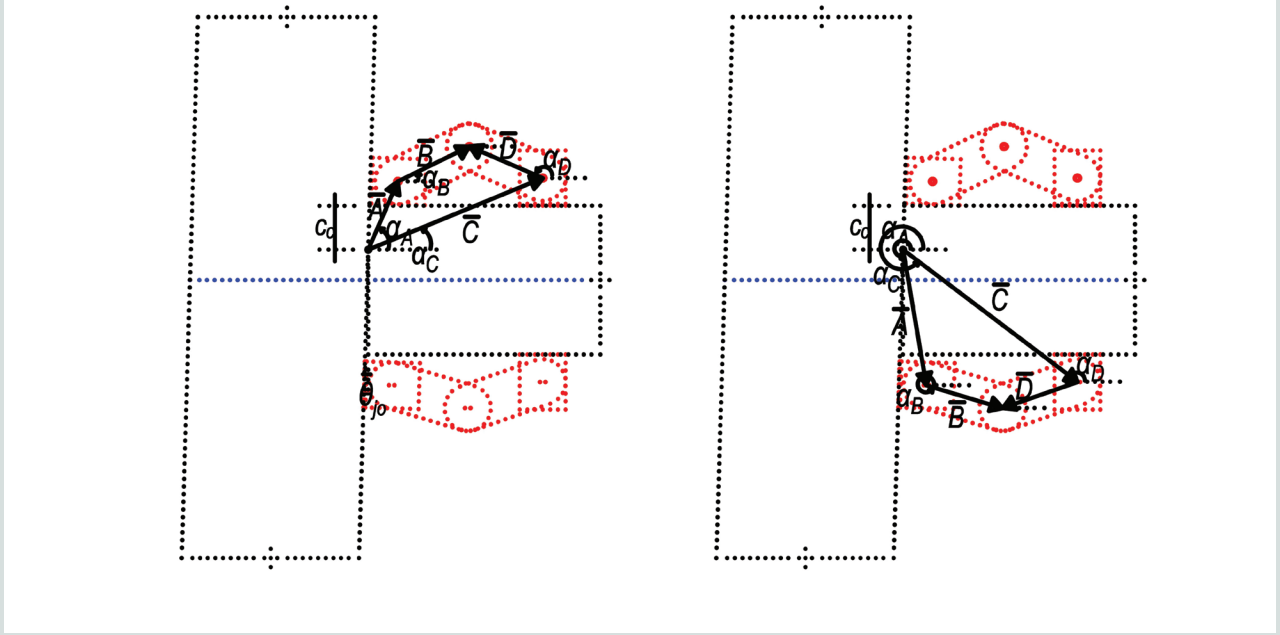

Figure 15. Kinematics of the damper system. Note: $\overline{A}$ = magnitude of vector A; $\overline{B}$ = magnitude of vector B; c_c = distance between extreme compression fiber to the origin of rotation at the beam-column joint; $\overline{C}$ = magnitude of vector C; $\overline{D}$ = magnitude of vector D; α_A = angle between vector A and positive x axis; α_B = angle between vector B and positive x axis; α_C = angle between vector C and positive x axis; α_D = angle between vector D and positive x axis; θ_{jo} = maximum expected rotation at the precast concrete beam-column joint for kinematic analysis.

Acknowledgments

This work was funded by the Research Fund (grant number 21AD8) of Bogazici University. The assistance of the technical staff of Bogazici University Materials Lab, where the experiments were carried out, is greatly appreciated.

References

1. Priestley, N. M. J., S. Sritharan, J. R. Conley, and S. Pampanin. 1999. "Preliminary Results and Conclusions from the PRESSS Five-Story Precast Concrete Test Building." *PCI Journal* 44 (6): 42–67. https://doi.org/10.15554/pcij.11011999.42.67.

2. Sakata, H., and A. Wada. 2006. "Study on Damage Controlled Precast-Prestressed Concrete Structure with P/C Mild-Press-Joint-Part 2: Experimental Study on Mechanical Behavior of Frame with P/C Mild-Press-Joint". In *Second International fib Congress in Naples, Italy (2006)—Proceedings*. Lausanne, Switzerland: *fib* (International Federation for Structural Concrete).

3. Ertas, O., and S. Ozden. 2007. "Behavior of Unbonded, Post-tensioned, Precast Concrete Connections with Different Percentages of Mild Steel Reinforcement." *PCI Journal* 52 (2): 32–44. https://doi.org/10.15554/pcij.03012007.32.44.

4. Morgen, B. G., and Y. Kurama. 2004. "A Friction Damper for Post-tensioned Precast Concrete Moment Frames." *PCI Journal* 49 (4): 113–133. https://doi.org/10.15554/pcij.07012004.112.133.

5. Morgen, B. G., and Y. Kurama. 2007. *Friction-Damped Unbonded Post-Tensioned Precast Concrete Moment Frame Structures for Seismic Regions*. Structural engineering research report 113-133. Notre Dame, IN: Department of Civil Engineering and Geological Sciences, University of Notre Dame.

6. ACI (American Concrete Institute). 2001. *Acceptance Criteria for Moment Frames Based on Structural Testing*. ACI T1.1-01/T1.1R-01. Farmington Hills, MI: ACI.

7. Pampanin, S., A. Palermo, D. K. Bull, and D. Marriott. 2008. "Dynamic Testing of Precast, Post-tensioned Rocking Wall Systems with Alternative Dissipating Solutions." *Bulletin of the New Zealand Society for Earthquake Engineering* 41 (2): 90–103. https://doi.org/10.5459/bnzsee.41.2.90-103.

8. Koshikawa, T., H. Kadowaki, and M. Matsumora. 2012. "Energy Dissipation Efficiency of Unbonded Post-tensioned Precast Concrete Beam–Column Connections with Beam-End Dampers." In *Proceedings of the Fifteenth World Conference on Earthquake Engineering, Lisbon, Portugal, 2012*. https://www.iitk.ac.in/nicee/wcee/article/WCEE2012_0812.pdf.

9. Koshikawa, T. 2017. "Moment and Energy Dissipation Capacities of Post-tensioned Precast Concrete Connections Employing a Friction Mechanism." *Engineering Structures* 138: 170–180. https://doi.org/10.1016/j.engstruct.2017.02.012.

10. Kalliontzis, D., and S. Sritharan. 2021. "Seismic Behavior of Unbonded Post-tensioned Precast Concrete Members with Thin Rubber Layers at the Jointed Connection." *PCI Journal* 66 (1): 60–76. https://doi.org/10.15554/pcij66.1-02.

11. Cai, X., N. Gong, C. C. Fu, Y. Zhu, and J. Wu. 2021. "Seismic Behavior of Self-Centering Prestressed Precast Concrete Frame Subassembly Using Steel Top and Seat Angles." *Engineering Structures*, no. 229, 111646. https://doi.org/10.1016/j.engstruct.2020.111646.

12. Li, Y., F. Gang, Y.Ding, and L. Wang. 2020. "Experimental and Numerical Study on Low-Damage Self-Centering Precast Concrete Frame Connections with Replaceable Dampers." *Engineering Structures*, no. 220, 111011. https://doi.org/10.1016/j.engstruct.2020.111011.

13. Zhang, C., H. Li, and W. Gao. 2020. "Development of a Novel Friction Damped Joint for Damage-Plasticity Control of Precast Concrete Walls." *Engineering Structures* 219: 110850. https://doi.org/10.1016/j.engstruct.2020.110850.

14. Wang, H., E. M. Marino, P. Pan, H. Liu, and X. Nie. 2018. "Experimental Study of a Novel Precast Prestressed Concrete Beam-to-Column Joint." *Engineering Structures*, no. 156, 68–81. https://doi.org/10.1016/j.engstruct.2017.11.011.

15. Li, Z., Y. Qi, and J. Teng. 2020. "Experimental Investigation of Prefabricated Beam-to-Column Steel Joints for Precast Concrete Structures Under Cyclic Loading." *Engineering Structures*, no. 209, 110217. https://doi.org/10.1016/j.engstruct.2020.110217.

16. Nazari, M., and S. Sritharan. 2019. "Seismic Design of Precast Concrete Rocking Wall Systems with Varying Hysteretic Damping." *PCI Journal* 64 (5): 58–76. https://doi.org/10.15554/pcij64.5-04.

17. Constantinou M., P. Tsopelas, W. Hammel, and A. N. Sigaher. 2001. "Toggle-Brace-Damper Seismic Energy Dissipation Systems." *Journal of Structural Engineering* 127 (2): 105–112. https://doi.org/10.1061/(ASCE)0733-9445(2001)127:2(105).

18. Hwang, J.-S., K. Jinkoo, and Y. Kim. 2007. "Rotational Inertia Dampers with Toggle Bracing for Vibration Control of a Building Structure." *Engineering Structures* 29 (6): 1201–1208. https://doi.org/10.1016/j.engstruct.2006.08.005.

19. Ribakov, Y., and A. M. Reinhorn. 2003. "Design of Amplified Structural Damping Using Optimal Considerations." *Journal of Structural Engineering* 129 (10): 1422–1427. https://doi.org/10.1061/(ASCE)0733-9445(2003)129:10(1422).

20. Zhang, R., H. He, D. Weng, H. Zhou, and S. Ding. 2012. "Theoretical Analysis and Experimental Research on Toggle-Brace-Damper System Considering Different Installation Modes." *Scientia Iranica* 19 (6): 1379–1390. https://doi.org/10.1016/j.scient.2012.10.011.

21. Berton, S., and J. E. Bolander. 2005. "Amplification System for Supplemental Damping Mechanisms in Seismic Applications." *Journal of Structural Engineering* 131 (6): 979. https://doi.org/10.1061/(ASCE)0733-9445(2005)131:6(979).

22. Huang, H. C. 2009. "Efficiency of the Motion Amplification Mechanism with Viscous Dampers and Its Application in High-Rise Buildings." *Earthquake Engineering and Engineering Vibration*, no. 8, 521–536. https://doi.org/10.1007/s11803-009-9116-2.

23. Londoño, J. M, S. A. Neild, and D. J. Wagg. 2015. "Using a Damper Amplification Factor to Increase Energy Dissipation in Structures." *Engineering Structures* 84 (1): 162–171. https://doi.org/10.1016/j.engstruct.2014.11.019.

24. Mualla, I. 2000. "Experimental Evaluation of New Friction Damper Device." In *Proceedings of the Twelfth World Conference on Earthquake Engineering, Auckland, New Zealand*. https://www.iitk.ac.in/nicee/wcee/article/1048.pdf.

25. Anuoshehei M., F. Daneshjoo, S. Mahboubi, and M. A. Hashemi. 2018. "Empirical Evaluation of Cyclic Behavior of Rotational Friction Dampers with Different Metal Pads." *Scientia Iranica* 25 (6): 3021–3029. https://doi.org/10.24200/sci.2017.4225.

26. Jarrahi, H., A. Asadi, M. Khatibinia, and S. Etedali. 2020. "Optimal Design of Rotational Friction Dampers for Improving Seismic Performance of Inelastic Structures." *Journal of Building Engineering*, no. 27, 100960. https://doi.org/10.1016/j.jobe.2019.100960.

27. FEMA (Federal Emergency Management Agency). 2000. *Prestandard and Commentary for the Seismic Rehabilitation of Buildings*. FEMA-356. Washington, DC: FEMA. https://www.nehrp.gov/pdf/fema356.pdf.

28. Latour, M., V. Piluso, and G. Rizzano. 2014, "Experimental Analysis on Friction Materials for Supplemental Damping Devices." *Construction and Building Materials*, no. 65, 159–176. https://doi.org/10.1016/j.conbuildmat.2014.04.092.

Notation

A_h = total area of hysteresis loop

A_{ps} = total cross-sectional area of one layer of post-tensioning strands

$\overline{A}$ = magnitude of vector A

$\overline{B}$ = magnitude of vector B

c_c = distance between extreme compression fiber to the origin of rotation at the beam-column joint

$\overline{C}$ = magnitude of vector C

d = relative translational displacement

d_{blt} = diameter of bolt

d_i = relative translational displacement at damper component *i*

d_1 =relative translational displacement at damper component 1

d_2 = relative translational displacement at damper component 2

d_3 = relative translational displacement at damper component 3

$\overline{D}$ = magnitude of vector D

E_a = modulus of elasticity of aluminum

E_b = modulus of elasticity of bolt

E_s = modulus of elasticity of structural steel

E_1 = peak lateral resistance for positive loading for the relevant sequence

E_2 = peak lateral resistance for negative loading for the relevant sequence

f_{ua} = tensile strength of aluminum

f_{ub} = tensile strength of bolt

f_{us} = tensile strength of structural steel

f_{ya} = yield strength of aluminum

f_{yb} = yield strength of bolt

f_{ys} = yield strength of structural steel

F = total vertical force acting on the damper

F_b = force acting on beam end

F_{max} = maximum force capacity of the test specimen

F_r = maximum force capacity of the subassembly at the given drift ratio

F_1 = vertical force at the left component of the damper

F_2 = vertical force at the right component of the damper

K = constant for bolt material and size

K_i = initial stiffness

n = number of friction surfaces

N_b = clamping force acting on the bolt due to applied torque

p = stress acting on the friction surface

r_1 = inner radius of the friction surface

r_2 = outer radius of the friction surface

T_{blt} = bolt torque

$T_{blt,m}$ = bolt torque applied to the middle joint in experiments

$T_{blt,tb}$ = bolt torque applied to the top and bottom joints in experiments

T_{fr} = frictional clamping torque value applied to the surface of all damper joints for subassembly analyses

u = axial deformation

u_i = axial deformation of yielding damper component *i*

u_{max} = displacement amplitude (maximum displacement) for experiments

$u(t)$ = vertical displacement imposed at the top joint of damper at time *t*

u_1 = axial deformation of yielding damper component 1

u_2 = axial deformation of yielding damper component 2

u_3 = axial deformation of yielding damper component 3

W_D = work done by the closed loop under force versus the displacement relationship

$W_{D,avg}$ = average area of hysteresis loop for all cycles

α_A = angle between vector A and positive x axis

α_B = angle between vector B and positive x axis

α_C = angle between vector C and positive x axis

α_D = angle between vector D and positive x axis

β = relative energy dissipation ratio defined by ACI T1.1-01

$\theta_{fr,1}^{(t)}$ = initial angle of the damper at time t

$\theta_{fr,1}^{(0)}$ = initial angle of the damper at time 0

θ_{imp} = imposed rotation at the precast concrete beam-column joint

θ_{jo} = maximum expected rotation at the precast concrete beam-column joint for kinematic analysis

μ = coefficient of friction between surfaces

About the authors

Ahmet Ata Kulaksizoglu, PhD, is a structural engineer. He received his bachelor of science from State University of New York at Buffalo and his master of science and doctorate degree from Bogazici University in Istanbul, Turkey. His research interests include computational structural engineering, precast concrete, and post-tensioned concrete.

Cetin Yilmaz, PhD, is a professor of mechanical engineering at Bogazici University in Istanbul, Turkey. He received his bachelor of science from Bogazici University and his master of science and doctorate degree from the University of Michigan. His research interests include vibration isolation and mechanical design.

Cem Yalcin, PhD, PEng, is a professor of civil engineering at Bogazici University in Istanbul, Turkey. He received his bachelor of science from Bogazici University, his master of science from Technical University of Nova Scotia, and his doctorate degree from the University of Ottawa. His research interests include experimental methods of concrete structures, seismic retrofitting, bridge engineering, precast concrete structures, and prestressed concrete structures.

Abstract

This paper describes research on the behavior of precast, post-tensioned concrete rocking systems with a proposed new type of external rotational friction damper. The proposed damper takes advantage of geometrical arrangement with small initial angle (less than 20 degrees) to amplify the relative rotations due to the unique gap opening mechanism that occurs in the joints of these systems. These relative rotations, which take place on friction surfaces between metallic friction plates, contribute to the energy dissipation and force capacity of the system by means of rotational friction. The novelty of the proposed damper stems from the amplification effect, which provides substantial energy dissipation capacity even in small drift demands. In this study, a numerical model was developed and verified with experimental results. This numerical model was used to analyze unbonded, post-tensioned beam-column subassemblies and frames with and without the proposed damper tested to develop the force-displacement relations. The analysis results indicate that the proposed damper would effectively dissipate seismic energy and increase force capacity.

Keywords

Frictional damping, low-damage seismic system, precast concrete seismic structural system, seismic design, unbonded post-tensioned precast concrete.

Review policy

This paper was reviewed in accordance with the Precast/Prestressed Concrete Institute's peer-review process. The Precast/Prestressed Concrete Institute is not responsible for statements made by authors of papers in *PCI Journal*. No payment is offered.

Publishing details

This paper appears in *PCI Journal* (ISSN 0887-9672) V. 68, No. 6, November–December 2023, and can be found at https://doi.org/10.15554/pcij68.6-02. *PCI Journal* is published bimonthly by the Precast/Prestressed Concrete Institute, 8770 W. Bryn Mawr Ave., Suite 1150, Chicago, IL 60631.

Reader comments

Please address any reader comments to *PCI Journal* editor-in-chief Tom Klemens at tklemens@pci.org or Precast/Prestressed Concrete Institute, c/o PCI Journal, 8770 W. Bryn Mawr Ave., Suite 1150, Chicago, IL 60631.